Impact of Hot Carrier Stress on the Defect Density and Mobility in Double-Gated Graphene Field-Effect Transistors

Yu.Yu. Illarionov*†, M. Waltl*, A.D. Smith‡, S. Vaziri‡, M. Ostling‡, M.C. Lemme§ and T. Grasser*

* Institute for Microelectronics, TU Wien, Austria
† Ioffe Physical-Technical Institute, Russia
‡ KTH Royal Institute of Technology, Sweden
§ University of Siegen, Germany

***Abstract*—We study the impact of hot-carrier degradation (HCD) on the performance of graphene field-effect transistors (GFETs) for different polarities of HC and bias stress. Our results show that the impact of HCD consists in a change of both charged defect density and carrier mobility. At the same time, the mobility degradation agrees with an attractive/repulsive scattering asymmetry and can be understood based on the analysis of the defect density variation.**

I. Introduction

Graphene is a next-generation carbon material with outstanding physical and electrical properties [1, 2] and good compatibility with standard CMOS technology. Although several research groups have succeeded in fabricating graphene-based FETs (GFETs) [3, 4], only a few attempts have been made at trying to understand their reliability [5–7]. All these previous works are devoted to bias-temperature instabilities (BTI) but no analysis has been attempted with respect to hot-carrier degradation (HCD). We thus study the impact of HCD with different polarity of HC and bias components on the defect density and mobility in single-layer double-gated GFETs.

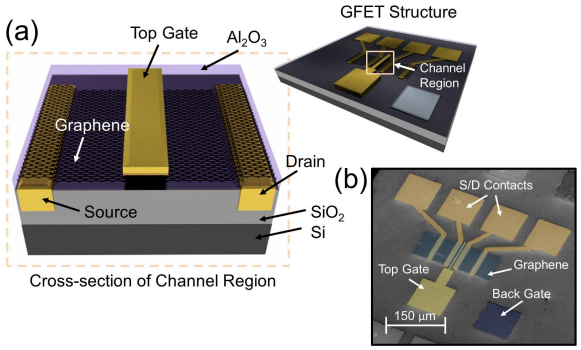

Fig. 1: a) Schematic layout of the double-gated single-layer GFET and a cross-section of the channel region (L=4 μm and W=20–80 μm). b) Top view of the double-gated GFET obtained using scanning-electron microscopy (SEM).

II. Devices

Double-gated GFETs with the graphene channel sandwiched between Al_2O_3 (top gate) and SiO_2 (back gate) were fabricated using a standard lithography process [9]. Their layout is given in Fig. 1. Initially, the devices have been treated by baking at T=300 °C in an H_2/He mixture which resulted in a significant decrease in variability [7]. As shown in our previous works [7, 10], our GFETs share all typical properties known from literature reports [5].

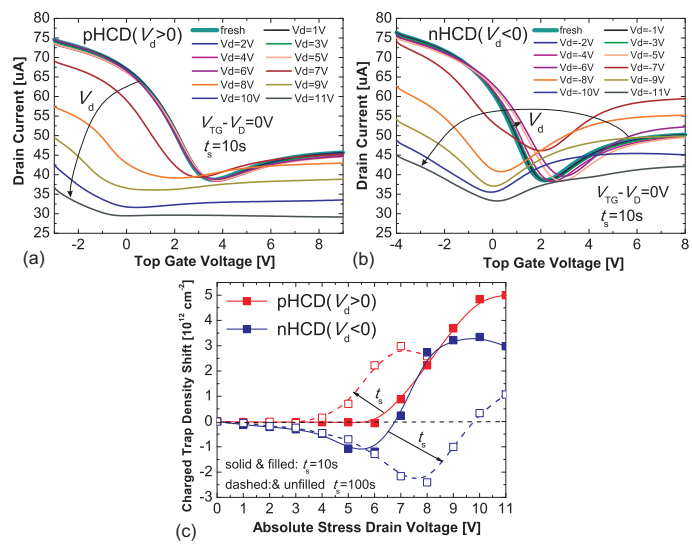

Fig. 2: a) Top gate transfer characteristics measured after subsequent stresses (t_s=10 s) with positive V_d and V_{TG}-V_D=0 (pHCD). b) Related results for negative V_d (nHCD). c) Variation of charged trap density shift $\Delta N_T = C_{ox}\Delta V_D/q$ for pHCD and nHCD, the results corresponding to t_s=10 s and 100 s are plotted. A pHCD stress is able to create only positively charged defects while an nHCD stress creates negatively charged defects at smaller V_d and positively charged ones at larger V_d. Interestingly, positively charged defects may tend to disappear after a stress with larger V_d, similarly to Si technologies [8].

III. Experiment

We analyze the transformation of the top gate transfer characteristics of GFETs which are known to be sensitive to the detrimental impact of the environment [6]. For this reason, all our measurements were performed in vacuum (10^{-5} torr). The impact of HCD and bias stress on the device performance was examined as follows: after measuring the reference transfer characteristic, a stress with constant top gate voltage V_{TG} and drain voltage V_d was applied for a certain stress time t_s; the back gate bias V_{BG} was kept at zero. Then the recovery of the stressed device was monitored for several hours after which a new stress with a larger V_d was applied.

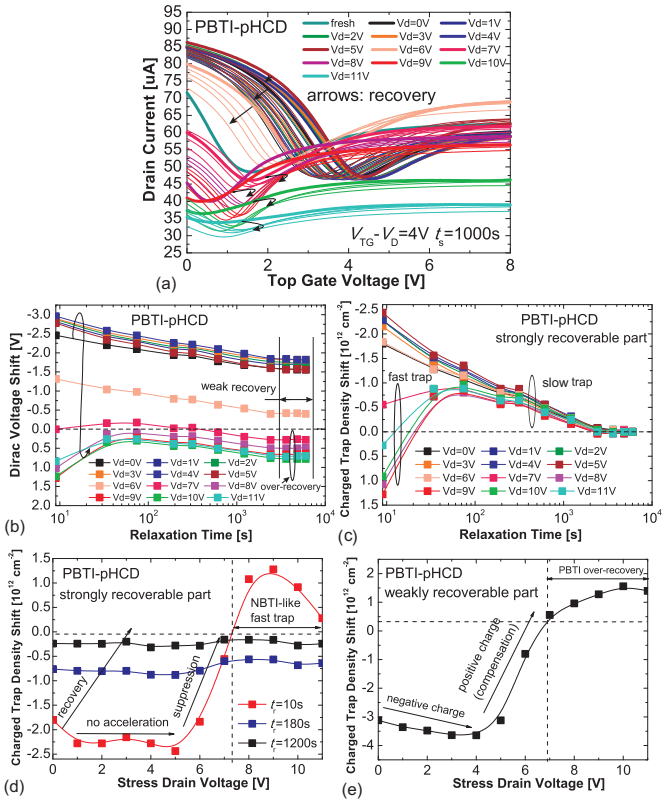

Fig. 3: a) Time evolution of the top gate transfer characteristics after subsequent PBTI-pHCD stresses. b) The corresponding V_D recovery traces contain both strongly recoverable (c,d) and weakly recoverable (e) components. At low V_d the former has a PBTI-like nature and thus is mainly associated with the bias stress, being almost independent of V_d. The presence of a strong V_d leads to a suppression of the strongly recoverable component and introduces NBTI-like fast trap behavior which is also typical for pure NBTI in GFETs [7]. Interestingly, the slow trap component remains PBTI-like (c). The weakly recoverable component (e) is associated with negatively charged defects created by PBTI at smaller V_d and with positive charge introduced by pHCD at larger V_d. The presence of an extra positive charge at larger stress V_d (e) leads to an over-recovery of PBTI-like degradation (b).

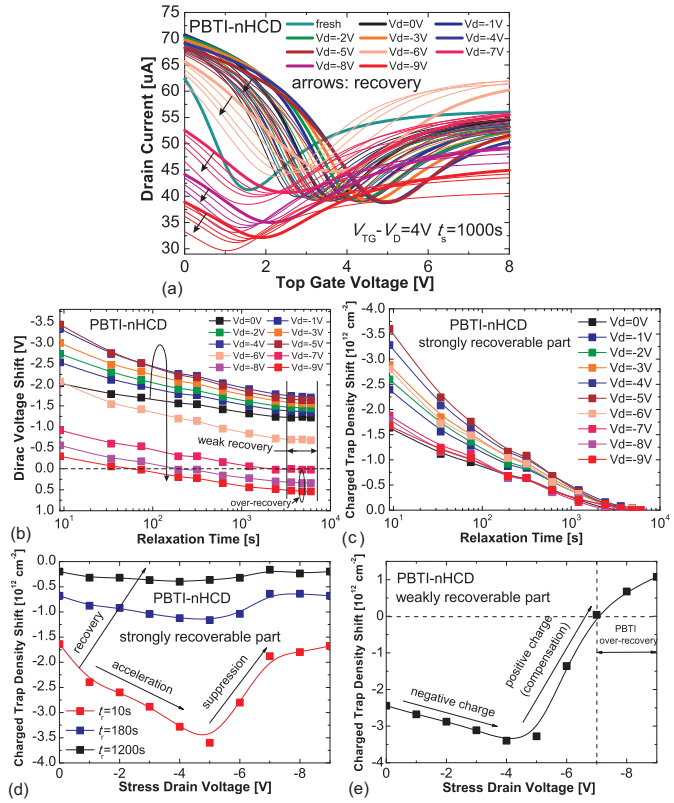

Fig. 4: a) Time evolution of the top gate transfer characteristics after subsequent PBTI-nHCD stresses. b) Contrary to Fig. 3, PBTI-like degradation at smaller V_d is significantly accelerated by nHCD which is able to create a negative charge. However, this is mainly associated with the strongly recoverable component (c,d). At larger V_d the strongly recoverable component is suppressed by nHCD but remains PBTI-like due to the presence of larger negative charge density (d), unlike Fig. 3. The weakly recoverable component (e) is similar to the previous case, although an increase of negative charge density obviously proceeds faster. The presence of an extra positive charge at larger V_d leads to over-recovery of PBTI (b).

In the spirit of our previous work [7], V_{TG}-$V_D(V_d) \approx$ const with V_D being the Dirac voltage was maintained in order to approximately keep the oxide field constant during all stress rounds. Also, in this work all the measurements have been performed at room temperature.

IV. Results and Discussions

In Fig. 2 the resulting transformation of the top gate transfer characteristics after alternating pure HCD (V_{TG}-V_D=0) stresses with increasing positive V_d (pHCD) and negative V_d (nHCD) is depicted. Clearly, the impact of HC stress on the device performance depends on the polarity of V_d. pHCD shifts V_D in an NBTI-like manner and also leads to a shape transformation and vertical drift of the transfer characteristics (Fig. 2a). However, nHCD is of PBTI-like nature at smaller V_d and NBTI-like at larger V_d while the transition at moderate V_d is associated with a current increase (Fig. 2b). Then we treat the Dirac point shift in terms of the charged trap density shift $\Delta N_T = C_{ox}\Delta V_D/q$ with C_{ox} being the top gate oxide capacitance and $\Delta V_D = V_D^{fresh}$-$V_D^{stressed}$. This allows us to conclude that pHCD leads to a creation of positively charged defects while nHCD introduces a negative charge at smaller V_d and a positive charge at larger V_d (Fig. 2c). An increase of t_s makes pHCD more pronounced while in the case of nHCD this leads to a stronger interplay between the two mechanisms. However, under real operation conditions the HC stress occurs in conjuction with the bias stress. Thus we proceed with the analysis of pHCD and nHCD overlaid on either positive (PBTI) or negative (NBTI) bias stress V_{TG}-V_D=±4V with t_s=1000s. In Fig. 3 the results for PBTI-pHCD are depicted. The degradation/recovery dynamics strongly correlate with the magnitude of the applied HC stress. At smaller V_d a PBTI-like shift of the Dirac point is observed which means that the impact of bias stress dominates. However, at larger V_d an NBTI-like pHCD first reduces the Dirac point shift and then introduces an NBTI-like fast trap shift which is similar to pure NBTI in GFETs [7]. The total ΔV_D (Fig. 3b) can be separated into strongly recoverable and weakly recoverable components; for convenience each of them is plotted in units of ΔN_T. The strongly recoverable component (Fig. 3c,d) at smaller V_d is mainly associated with bias stress while at larger V_d pHCD reduces it and also supplements an NBTI-like fast trap part. Interestingly, the slow trap part remains PBTI-like and thus originates from the bias stress independently of the HC stress magnitude. The weakly recoverable component (Fig. 3e) at smaller V_d originates from the bias stress and reflects the

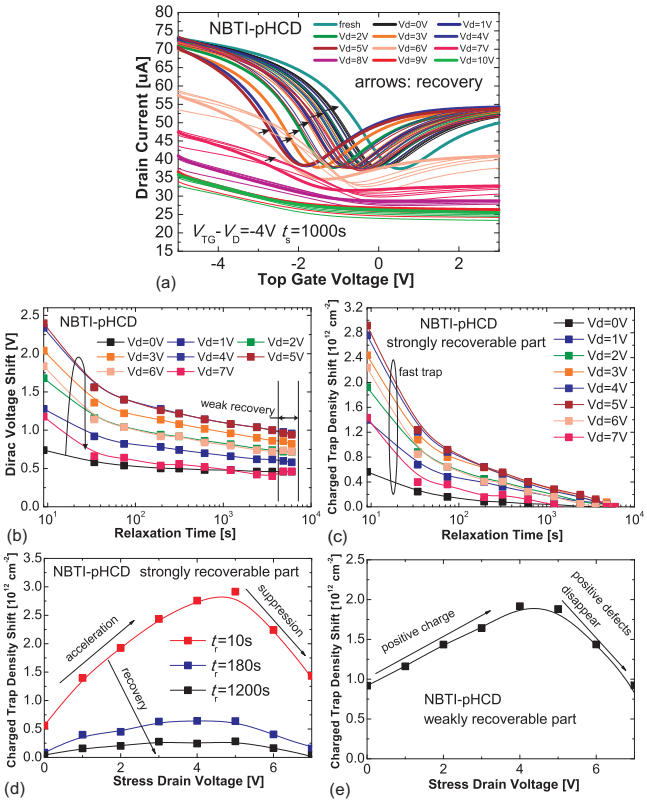

Fig. 5: a) Time evolution of the top gate transfer characteristics after subsequent NBTI-pHCD stresses. b) In constrast to the previous two cases, both the HC and the bias component create positively charged defects. Thus, the degradation/recovery dynamics are completely NBTI-like and the recovery traces contain some kinks associated with the fast trap component, similarly to pure NBTI in GFETs [7]. Interestingly, both strongly (c,d) and weakly (e) recoverable components have similar behavior versus V_d. At smaller V_d they increase, showing that the HC and the bias components create defects of the same sign. However, at larger V_d the degradation in terms of ΔN_T becomes less pronounced which hints at disappearing of some positively charged defects, similarly to Si technologies [8]. Also, strong transformation of the curve shape does not allow a reliable extraction of ΔV_D for the largest V_d.

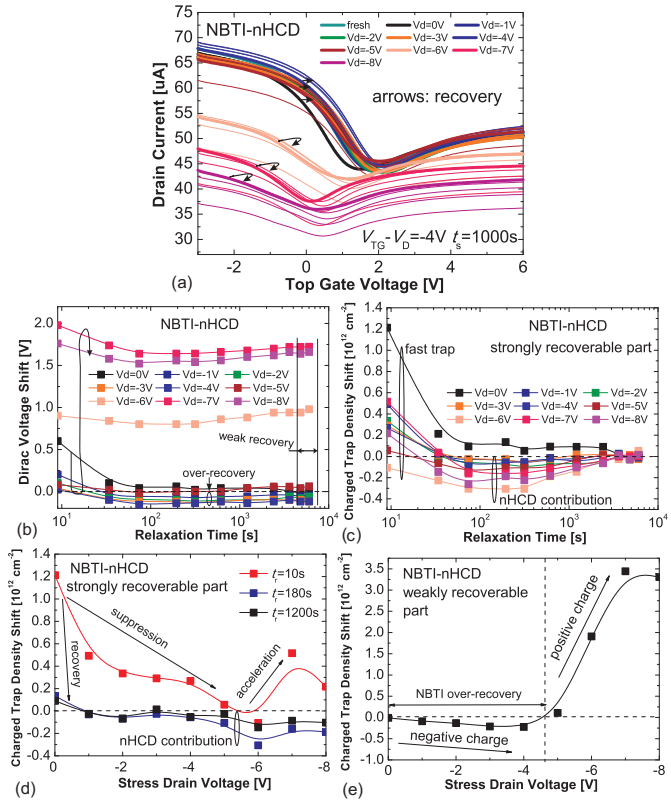

Fig. 6: a) Time evolution of the top gate transfer characteristics after subsequent NBTI-nHCD stresses. b) At smaller V_d NBTI-like degradation is suppressed by the nHCD component which creates negatively charged defects. However, at larger V_d an NBTI-like degradation is observed, because both the HC and the bias component create positively charged defects. The strongly recoverable component (c,d) for all non-zero V_d consists of an NBTI-like fast trap and PBTI-like contribution of nHCD (slow trap). The presence of the latter at larger V_d means that nHCD is able to create some negatively charged defects even at large V_d. The weakly recoverable component is contributed by nHCD-induced negative charge at smaller V_d and positive charge created by both the HC and the bias component at larger V_d. The former is not very significant and thus leads to a slight over-recovery of NBTI-like degradation.

presence of negative charge which is then compensated by pHCD at larger V_d. Moreover, an extra positive charge appears after the strong HC stresses which leads to over-recovery of PBTI-like degradation. The related results for PBTI-nHCD are plotted in Fig. 4. A PBTI-like nature of the nHCD component at smaller V_d results in a significant acceleration of the PBTI degradation while its NBTI-like nature at larger V_d leads to its suppression. However, contrary to the previous case, a more significant negative charge density avoids a complete suppression of the PBTI-like behavior. Thus, the strongly recoverable component remains PBTI-like within the whole V_d range and no NBTI-like fast trap appears (Fig. 4c,d). The behavior of the weakly recoverable component (Fig. 4e) is similar to PBTI-pHCD, although an increase of negative charge density obviously proceeds faster.

In particular, an extra positive charge leading to over-recovery of PBTI-like degradation is present at larger V_d. In Fig. 5 one can see the results for NBTI-pHCD. Obviously, in this case both the HC and the bias component are able to create only positively charged defects. Thus the degradation is NBTI-like within the whole V_d range and no over-recovery is observed (Fig. 5b).

However, a strong transformation of the shape of the characteristics (Fig. 5a) does not allow to perform a reliable extraction of ΔV_D for the largest V_d. The strongly recoverable component (Fig. 5c,d) initially increases versus V_d and shows the presence of an NBTI-like fast trap shift. But the stresses with larger V_d lead to a decrease of the degradation which indicates that positively charged defects disappear, similarly to Si technologies [8]. The weakly recoverable component (Fig. 5e) behaves versus V_d in the same manner which suggests the absence of any interplay in the considered case. Fig. 6 presents the related results for NBTI-nHCD. In this case the bias stress is suppressed by the PBTI-like nHCD component at smaller V_d and becomes significantly pronounced at larger V_d when nHCD is NBTI-like. Interestingly, in all cases except $V_d=0$ (pure NBTI) the strongly recoverable component (Fig. 6c,d) in addition to the NBTI-like fast trap contains a PBTI-like slow trap contribution which is obviously associated with nHCD. This means that despite the overall NBTI-like nature at larger V_d nHCD creates some negatively charged defects. The weakly recoverable component (Fig. 6e) at smaller V_d is associated with an insignificant amount of negative charge which leads to over-recovery of NBTI-like degradation. At larger V_d the

positive charge results in an incomplete recovery. However, all the degradation mechanisms considered above also lead to a mobility change. The mobility can be estimated using the transcondactance G_m measured in the linear regions of the transfer characteristics [11] (Fig. 7, inset); for unstressed devices $\mu_h = 90–150\,cm^2/Vs$ and $\mu_e = 20–60\,cm^2/Vs$.

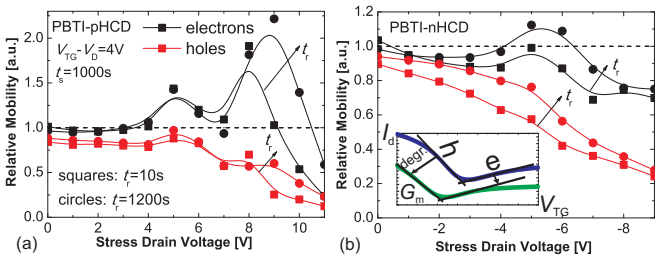

Fig. 7: Relative mobility versus V_d for PBTI-pHCD (a) and PBTI-nHCD (b). At smaller V_d the degradation of hole mobility is stronger than for electrons due to the presence of negative charge, leading to an attractive/repulsive scattering asymmetry [12]; screening effects increase the electron mobility at moderate V_d. At the same time, for PBTI-pHCD screening becomes more pronounced after the recovery of the NBTI-like fast traps, since the concentration of positive charge decreases. The inset sketches the mobility estimation procedure.

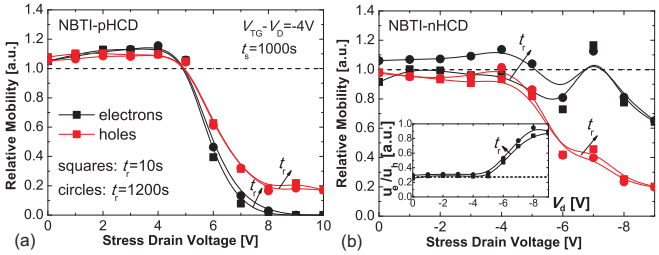

Fig. 8: Relative mobility versus V_d for NBTI-pHCD (a) and NBTI-nHCD (b). At smaller V_d the created charge is insufficient for a mobility degradation. At larger V_d the degradation of electron and hole mobility is nearly symmetric in the case of NBTI-pHCD which suggests that scattering at neutral imperfections dominates [12, 13]; the slight difference is due to the presence of positively charged defects. For NBTI-nHCD screening of positive charge prevents degradation of electron mobility and increases μ_e/μ_h (inset).

In Fig. 7 the relative mobility versus V_d is depicted for PBTI-pHCD and PBTI-nHCD. In both cases a negative charge is present at smaller V_d and the scattering is attractive for holes and repulsive for electrons. The former is known to be stronger than the latter [12] and thus the degradation of hole mobility is more significant. At moderate V_d a small amount of positive charge is either screened [13] or leads to screening of the remaining negative charge. Thus the electron mobility has a maximum. Interestingly, in the case of PBTI-pHCD there are two maxima: the first one corresponds to the beginning of charge compensation and the second one appears near the transition point and significantly increases after the recovery of the fast trap component (cf. Fig. 3d,e). The latter indicates that the positive charge introduced by the fast traps contributes to the attractive scattering of electrons. Since the negative charge concentration for PBTI-pHCD is smaller than for PBTI-nHCD, in the former case the hole mobility is also affected by screening effects. In Fig. 8 the related results for NBTI-pHCD and NBTI-nHCD are provided. In both cases the charge created at smaller V_d is insufficient for a significant mobility degradation. In the case of NBTI-pHCD, larger V_d causes a nearly symmetric decrease of the electron and hole mobilities. This suggests scattering at neutral imperfections [12, 13] which more likely substitute disappearing positive defects (cf. Fig. 5d,e). The results for NBTI-nHCD demonstrate that at moderate V_d the electron mobility is affected by screening, similarly to the first two cases. An increase in μ_e/μ_h (inset) also suggests screening while the initial value is close to the one predicted in [12].

V. Conclusions

The BTI-HCD dynamics for different polarities of HC and bias stress were analyzed. The impact of HCD consists in a variation of defect density and a mobility degradation. These two contributions correlate; knowledge of the charged trap density (sign and magnitude) allows to understand the mobility degradation which is consistent with the previously reported attractive/repulsive scattering asymmetry.

VI. Acknowledgements

The authors thank EC for the financial support through the STREP projects MORDRED (n° 261868) and GRADE (n° 317839), an ERC Starting Grant (InteGraDe, n° 307311), the German Research Foundation (DFG, LE 2440/1-1 and 2-1).

References

[1] A. Geim and K. Novoselov, "Numerical Methods for Semiconductor Device Simulation," *Nature Materials*, vol. 6, no. 3, pp. 183–191, 2007.
[2] V. Dorgan, M.-H. Bae, and E. Pop, "Mobility and saturation velocity in graphene on SiO2," *Applied Physics Letters*, vol. 97, p. 082112, 2010.
[3] M. Lemme, T. Echtermeyer, M. Baus, and H. Kurz, "A Graphene Field Effect Device," *IEEE Electron Device Letters*, vol. 28, no. 4, pp. 1–12, 2007.
[4] M. Engel, M. Steiner, A. Lombardo, A. Ferrari, H. Loehneysen, P. Avouris, and R. Krupke, "Light-matter Interaction in a Microcavity-controlled Graphene Transistor," *Nature Communications*, vol. 3, p. 906, 2012.
[5] S. Imam, S. Sabri, and T. Szkopek, "Low-Frequency Noise and Hysteresis in Graphene Field-Effect Transistors on Oxide," *Micro & Nano Letters*, vol. 5, no. 1, pp. 37–41, 2010.
[6] W. Liu, X. Sun, X. Tran, Z. Fang, Z. Wang, F. Wang, L. Wu, J. Zhang, J. Wei, H. Zhu, and H. Yu, "Observation of the Ambient Effect in BTI Characteristics of Back-Gated Single Layer Graphene Field Effect Transistors," *IEEE Trans.Electron Devices*, vol. 60, no. 8, pp. 2682–2686, 2013.
[7] Y. Illarionov, A. Smith, S. Vaziri, M. Ostling, T. Mueller, M. Lemme, and T. Grasser, "Bias-Temperature Instability in Single-Layer Graphene Field-Effect Transistors," *Appl.Phys.Lett.*, vol. 105, p. 143507, 2014.
[8] T. Grasser, P.-J. Wagner, H. Reisinger, T. Aichinger, G. Pobegen, M. Nelhiebel, and B. Kaczer, "Analytic Modeling of the Bias Temperature Instability Using Capture/Emission Time Maps," in *IEDM*, Dec. 2011, pp. 27.4.1–27.4.4.
[9] S. Vaziri, G. Lupina, A. Paussa, A. D. Smith, C. Henkel, G. Lippert, J. Dabrowski, W. Mehr, M. Östling, and M. Lemme, "A Manufacturable Process Integration Approach for Graphene Devices," *Solid-State Electron.*, vol. 84, pp. 185–190, 2013.
[10] Y. Illarionov, A. Smith, S. Vaziri, M. Ostling, T. Mueller, M. Lemme, and T. Grasser, "Bias-temperature Instability in Single-layer Graphene Field-effect Transistors: a Reliability Challenge," in *IEEE SNW*, 2014, pp. 29–30.
[11] G. Venugopal, K. Krishnamoorthy, and S. Kim, "Investigation of Transfer Characteristics of High Performance Graphene Flakes," *J. Nanoscience & Nanotechnology*, vol. 13, pp. 3515–3518, 2013.
[12] D. Novikov, "Numbers of Donors and Acceptors from Transport Measurements in Graphene," *Appl.Phys.Lett.*, vol. 91, p. 102102, 2007.
[13] M. Katsnelson and K. Novoselov, "Graphene: New Bridge between Condensed Matter Physics and Quantum Electrodynamics," *Solid State Comm.*, vol. 143, pp. 3–13, 2007.